STUDY ON AGEING OF COBALT FERRITE NANOPARTICLES AND THEIR FATE IN THE ENVIRONMENT

L. POPESCU[1], D. BUZATU[2], M. BALASOIU[3,4,5,] C. STAN[2], B. S. VASILE[6], L. SACARESCU[7], D. CREANGA[1]*, O. IVANKOV[3,5,8], D. SOLOVIOV[3,5,8], A.-M. BALASOIU-GAINA[3,9,10]

[1] "Alexandru Ioan Cuza" University, Faculty of Physics, Iasi, Romania, *mdor@uaic.ro
[2] "Politehnica" University of Bucharest, Physics Department, Faculty of Applied Sciences, Romania
[3] Joint Institute for Nuclear Research, Dubna, Russia
[4] "Horia Hulubei" Institute of Physics and Nuclear Engineering, Bucharest, Romania
[5] Moscow Technical Physics Institute, Dolgoprudnyi, Russia
[6] "Politehnica" University of Bucharest, Faculty of Applied Chemistry and Materials Science, Romania
[7] "Petru Poni" Institute of Macromolecular Chemistry, Iasi, Romania
[8] Institute for Safety Problems of Nuclear Power Plants of Ukrainian NAS, Kyiv, Ukraine
[9] CMCF, Moscow State University, Moscow, Russian Federation
[10] West University of Timisoara, Timisoara, Romania

Received January 14, 2019

Abstract. The stability in time is a critical feature of magnetic nanoparticles in aqueous suspensions, straightly related to the usability in various biomedical fields. This study was focused on the granularity features of cobalt ferrite nanoparticles, dispersed in water by using as stabilizer shell either citrate ions or oleate ones, since fine granulation confers time stability. Microstructural properties investigation was carried out by X-ray diffractometry, Transmission Electron Microscopy, Atomic Force Microscopy and Small Angle Neutron Scattering. The changings of internal organization of colloidal nanosystems during one-year ageing, with differences between the two stabilizer molecular shells, were revealed by microscopy imaging. Two mathematical fittings of Small Angle Neutron Scattering data provided results in accord with microscopy ones for the aged samples. The differences in the bioimpact of the two aged diluted magnetizable fluids on *Zea mays* plantlets during early ontogenetic stages were analyzed by photosynthesis pigment assay, considering final release of used nanoparticles in the environmental waters, air and soil.

Key words: cobalt ferrite nanoparticles, aged suspension stability, environmental impact.

1. INTRODUCTION

First *magnetic nanoparticles* (MNPs) in stable oily suspensions [1–3] were intended for technical purposes like dynamic sealing, heat dissipation, doping of technological materials, novel pumps, energy conversion devices, and other applications. They were designed as dense colloids with ferrophase consisting in metallic cores coated in oleic acid and dispersed in non-polar fluids such as hydrocarbons that do

not attack metallic device surfaces. This is basically the project of Massart for the nanosized magnetite precipitation and further stabilization in oily media [4].

Later, various applications in biomedicine were designed like cell separation, magnetocytolysis, drug delivery, tumor hyperthermia treatment, increasing contrast in MRI screening, decreasing implant infection and increasing tissue growth, cell manipulation, DNA sequencing. In the latter cases, where water was required to be the dispersion fluid, the resulted ferrophase suspensions are conveniently diluted for the supply in the body fluids. Organic molecules with hydrophilic character had to be used for metallic cores coating such as citric acid, lauric acid, starch, dextrans, amino-acids or various polymers all being able to ensure nanoparticle floating in water [5–12]. The stability of water based MNP suspensions became a peculiar issue mainly because of attraction forces between magnetic dipoles but also because of electrical interactions – that occur also for other, non-magnetic nanoparticles [13]. Consequently, the researcher needs to keep in mind that nanoparticle in fluid dispersions often aggregate, *i.e*. they tend to generate clusters, because of attraction forces of different nature, leading to the settling down of conglomerations. Hence, MNP dispersion can be used as-is, or diluted with suitable, compatible solvents; because nanoparticles settling down can affect the dispersions properties during storage, they can be mixed before use.

Magnetic nanoparticles can be synthesized by chemical method [4] through the conversion of metal salts into hydroxides and further transformation of hydroxides into mixed metal iron oxides. To remove unreacted reagents, ferrophase washing can be carried out with hot deionized water, diluted hydrochloric acid, ethanol, acetone or others. The residual products removal is important also for the ensuring of clean surface of nanoparticles for further interaction with surfactant stabilizer molecules.

After MNP aqueous suspension use in exploring or healing living organisms, the delivery in the environment *via* body fluids raise the challenge of magnetic contamination and nanotoxicity. Waste waters, soils and air flows are able to carry MNPs toward plants and beneficial microorganisms from the environment interfering with their metabolism [14–16]. In [14] the authors reported various bioeffects of different types of nanoparticles in vegetable organisms. However, the corresponding mechanisms remained a wide challenge for scientists. In [15] the bioeffects dependence on plant species, and on the nanoparticle properties (chemical composition, size and size distribution, magnetic properties etc.) was underlined. In [16] the influence of metal nanoparticles on the plant photosynthetic systems was discussed. In [17] the effect of magnetite nanoparticles on yield of maize was analyzed, being known that iron deficiency can be the cause of chlorotic or yellowed interveinal areas with consequences on crop quality [18].

This study might be of interest not only for the stability of magnetic nanoparticle suspensions intended for biomedical use but also for the further surveying of their fate in the environment where they are released.

2. THEORETICAL APPROACH OF THE STABILITY OF COLLOIDAL PARTICLE

The physico-chemical stability [13] concerns the balance of forces generated by: (i) external magnetic field gradient; (ii) gravitational field; (iii) magnetic dipole-dipole vicinity.

(i) In an external magnetic field gradient, the stability of MNP dispersion is favored by a high ratio of thermal energy to the magnetic energy:

$$\frac{k_B T}{(\mu_0 MHV)} \geq 1 \tag{1}$$

where k_B is Boltzmann's constant, T is the absolute temperature, μ_0 is the permeability of the free space, M is the magnetization, V is the particle volume and H is the magnetic field intensity. Thus, the maximum particle diameter, D, needs to satisfy the condition:

$$D < \left(\frac{k_B T}{\pi \mu_0 MH} \right)^{\frac{1}{3}} \tag{2}$$

Considering pure magnetite particles with M and H having approximate values of 4.46×10^5 A/m and 8×10^4A/m [13], in the magnetic field gradient of a hand made permanent magnet at room temperature (298 K), relation (2) gives a value of $D \leq 12$ nm.

(ii) Compared to the magnetic energy, $\mu_0 MH$, the gravitational attraction per unit volume of the MNP suspension contained within a laboratory vial of length $L = 5$ cm, *i.e.* $\Delta\rho Lg$ (where g is the gravitational constant of 9.8 m/s^2), is less than 0.05 (since $\Delta\rho = \rho_{solid} - \rho_{liquid}$), is approximately 4,300 kg/m^3 in the case of magnetite MNPs [13]. Thus, the stability against gravitational attraction is practically assured for pure magnetite MNPs.

(iii) Stability against dipole-dipole attraction involves a high ratio of thermal energy to the magnetic dipole energy:

$$\frac{k_B T}{\left(\frac{M^2 D_M^3 \pi \mu_0}{9 \left(\frac{2S}{D_M} + 2 \right)^3} \right)} \geq 1 \tag{3}$$

where D_M is the magnetic core diameter and s is the surface-to-surface separation distance.

When the particles are in tight contact, then $s = 0$ and the above condition become: $k_B T / (M^2 V \mu_0 / 12) \geq 1$. Consequently, for magnetite MNPs at room temperature:

$$D_M \leq \left[\frac{72 k_B T}{M^2 \pi \mu_0} \right]^{\frac{1}{3}} \tag{4}$$

resulting in $D_M < 7.8$ nm.

Thus, one may conclude that in the cases where the diameter of the MNP core of colloidal dispersion is $D < 10$ nm, a stable suspension is expected.

Since Van der Waals forces also occur, the role of the non-magnetic surfactant shell is very important for the colloidal MNP dispersion, although the chemical or physical combination with the ions from ferrophase surface increases the colloidal particle diameter by simultaneous diminution of the magnetic core.

3. EXPERIMENTAL

3.1. SAMPLE SYNTHESIS AND DISPERSION IN WATER

The MNP suspensions studied in this paper were synthesized by chemical co-precipitation in alkali medium (NaOH 25%) from stoichiometric (2:1) amounts of hydrated ferric chloride: $FeCl_3 \times 6H_2O$, and Co(II) sulfate: $CoSO_4$ that were purchased from Sigma-Aldrich, Lachner and Merck; all solutions (Table I) of metal salt precursors were prepared with deionized water (18.2 MΩ/cm, Barnstead EasyPureII purification device).

Table 1

Reagents and products

Sample	Ferric chloride	Cobalt sulfate	Sodium hydroxide	Core	Shell
CoFe-CA	3.62g, 134 mM	1.88g, 67 mM	50 mL, 1.7 M	$CoFeO_4$	1.7 g $C_6H_8O_7$
CoFe-SO	3.62g, 134 mM	1.88g, 67 mM	50 mL, 1.7 M	$CoFeO_4$	0.3g $C_{18}H_{33}NaO$

Surfactant shell was get using citric acid ($C_6H_8O_7$) and sodium oleate ($C_{18}H_{33}NaO$) from Sigma, that were used (Table 1) without further purification (adapted Massart method [19]).

The two volumes of iron and cobalt salts in solutions were vigorously mixed at over 80°C, then NaOH, heated at over 55°C was added carefully drop by drop;

magnetic stirring was continued for about 50 minutes. Citric acid (CA) was used to stabilize brownish ferrophase in water.

The procedure was repeated to get a second amount of ferrophase designed to be stabilized with sodium oleate (SO). The final products have been denoted as CoFe-CA (cobalt ferrite surfacted with citric acid) and respectively CoFe-SO (cobalt ferrite surfacted with sodium oleate) (Table 1). Nanoparticle coating with surfactant reagents was carried out at 80°C under mechanical stirring (1200 rpm), the surfactant excess being removed through repeated washings with 40°C deionized water.

3.2. CHARACTERIZATION METHODS

X-ray diffractometry (XRD) was carried out with Shimadzu LabX XRD-6000 (radiation Cu-K_α, λ = 1.5406 Å) from 20 to 80 degree with scanning speed of 0.1 degree/min.

Transmission Electron Microscopy (TEM), using Hitachi High-Tech HT7700 was applied with 0.20 nm resolution at 100 kV for the standard pole piece. Nanoparticle diameter was measured with ImageJ software.

Atomic Force Microscopy (AFM) scanning was accomplished with XE100, Park Systems, Silicon tips OMCL AC240TS, Olympus, 2 N/m spring constant, tip radius of cantilever $R < 10$ nm.

Small Angle Neutron Scattering (SANS) analysis – with YuMO spectrometer [20] in function at the high flux pulse IBR-2 reactor was performed at JINR Dubna, Russia. The experiments were carried out at sample-to-detector distances of 5.28 m and 13.04 m, resulting in a Q range of $0.007 \div 0.2$ Å^{-1} (Q being the scattering vector, $Q = (4\,\pi / \lambda)\sin(\theta / 2)$, where θ is the scattering angle and λ the wavelength associated to accelerated neutron beam). The Sonix+ software control system provides spectrometer operation [21]. FITTER Soft package and ATSAS (PRIMUS program) were used for experimental data interpretation [22].

3.3. BIOCHEMICAL ASSAY OF PHOTOSYNTHESIS PIGMENTS

Biological material was consistent with selected maize (*Zea mays* L.) caryopses that were let to germinate in darkness at 22.0 ± 0.5°C in INCUCELL device on watered porous paper support in adequate Petri dishes. Immediately after germination, the samples were daily supplied with 6–8 ml of each MNP suspension dilution ranging as: 20-40-60-80-100 µl/l. Fourteen old plantlets were analyzed, and the photosynthesis pigment contents in green tissue was assayed according to Lichtenhalter and Weiburn [23] based on 85% acetone extract and Shimadzu UV-Vis 1700 Pharma Spec device. The contents in chlorophyll A (*Chl A*), chlorophyll B (*Chl B*) and total carotene like pigments (*T.C.*) were assayed, being expressed as mg of pigment in the gram of fresh green tissue.

Three replies were carried out from each vegetal sample; coating shell controls were arranged by supplying the equivalent concentration of citric acid and respectively sodium oleate that corresponded to highest CoFe-CA and CoFe-SO MNP suspensions. Graphs were plotted with the average values and standard deviation bars.

4. RESULTS AND DISCUSSIONS

X-ray diffractometry evidenced inverse spinel crystallization system in both samples (Fig. 1 a, b) with all typical peaks according to PDF Card nr. 22-1086 [9].

Recorded data processing with usual Scherrer's formula [24] provided crystallite size (peak (311)) of around 11 nm in the case of CoFe-CA and about 10 nm in the case of CoFe-SO.

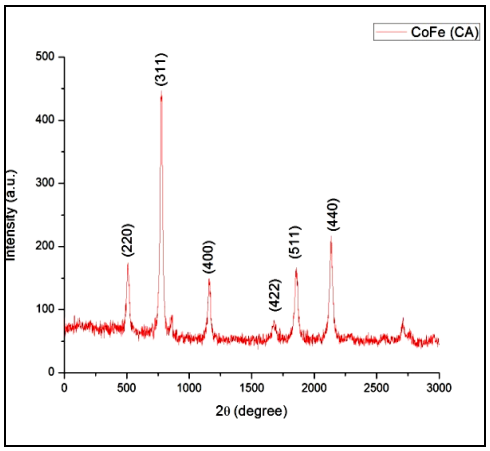

Fig. 1a – XRD for fresh CoFe-CA.

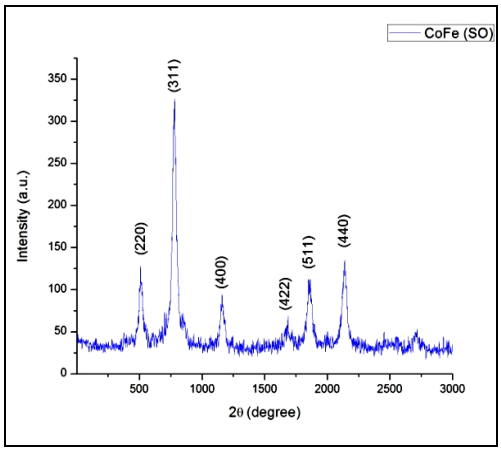

Fig. 1b –XRD for fresh CoFe-SO.

Quite similar XRD recordings were obtained for the freshly prepared and one-year aged samples, meaning that crystallinity properties remained unchanged during sample storage in environmental conditions. In contrast with thin citrate ion shell provided by citric acid, that confers mainly electrostatic stability of such colloidal nanoparticles, oleate ions arrange as double shell around metallic cores to result in hydrophilic coating and steric stabilization in water [25]. However, no additional peak could be identified for oleate suggesting that no ordered structures occurred for the coating shell of CoFe-SO MNPs, noting also that recording noise seems to be higher than for CoFe-CA MNPs. TEM investigation provided (Fig. 2 a, b) quasi-spherical grain images with polydispersity and mean values of about 20.2 nm for CoFe-CA MNPs, and respectively 23.1 nm for CoFe-SO MNPs.

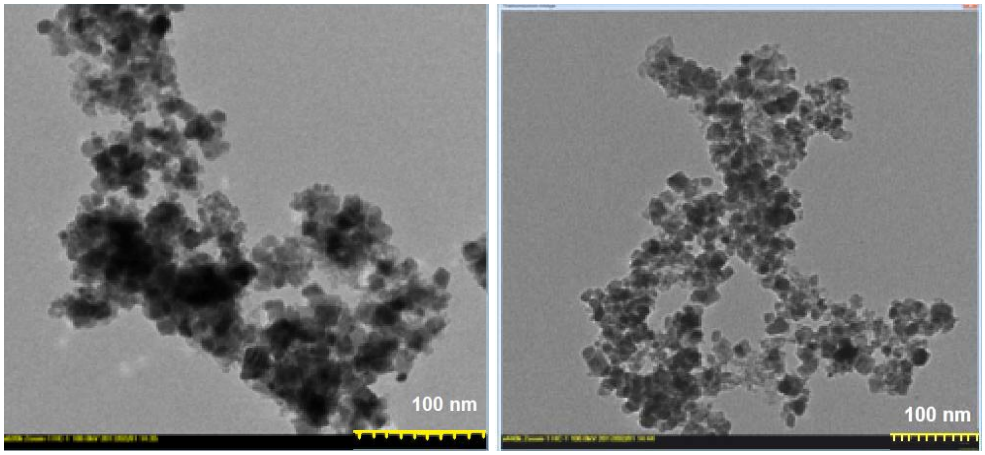

Fig. 2 – TEM recordings for freshly prepared suspensions:
a) left: CoFe-CA; b) right: CoFe-SO.

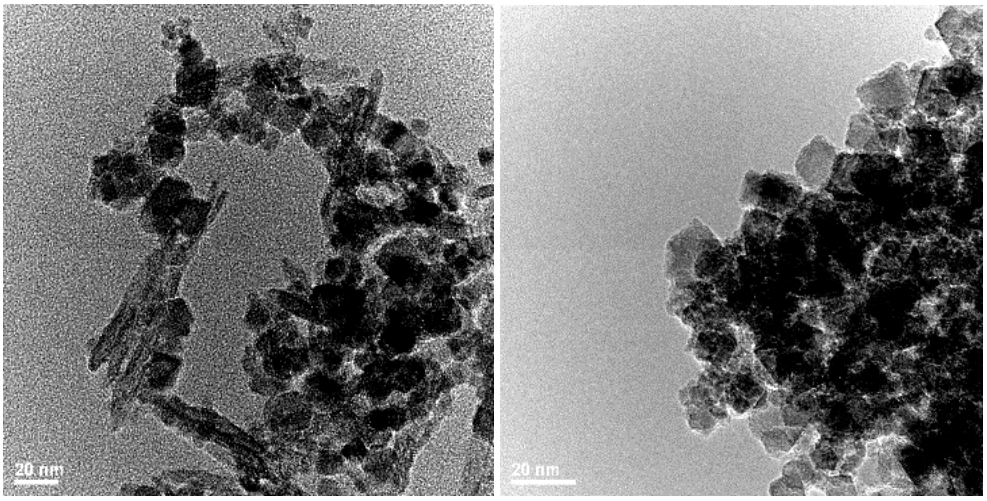

Fig. 3 – One year aged samples investigated by TEM:
a) left: CoFe-CA; b) right: CoFe-SO.

Some larger structures, as rather rare nanoparticle aggregates could be identified also but they could result from particle overlapping during TEM sample preparation by deposition on the grid support. Comparing with the theoretical stability limit it seems that the analyzed MNP suspensions are less stable than ideal ones or as oily nanoparticle suspensions – at least for long term storage.

Consequently, the granularity analysis was carried out one year later on the same samples that were stored in closed vials at room temperature.

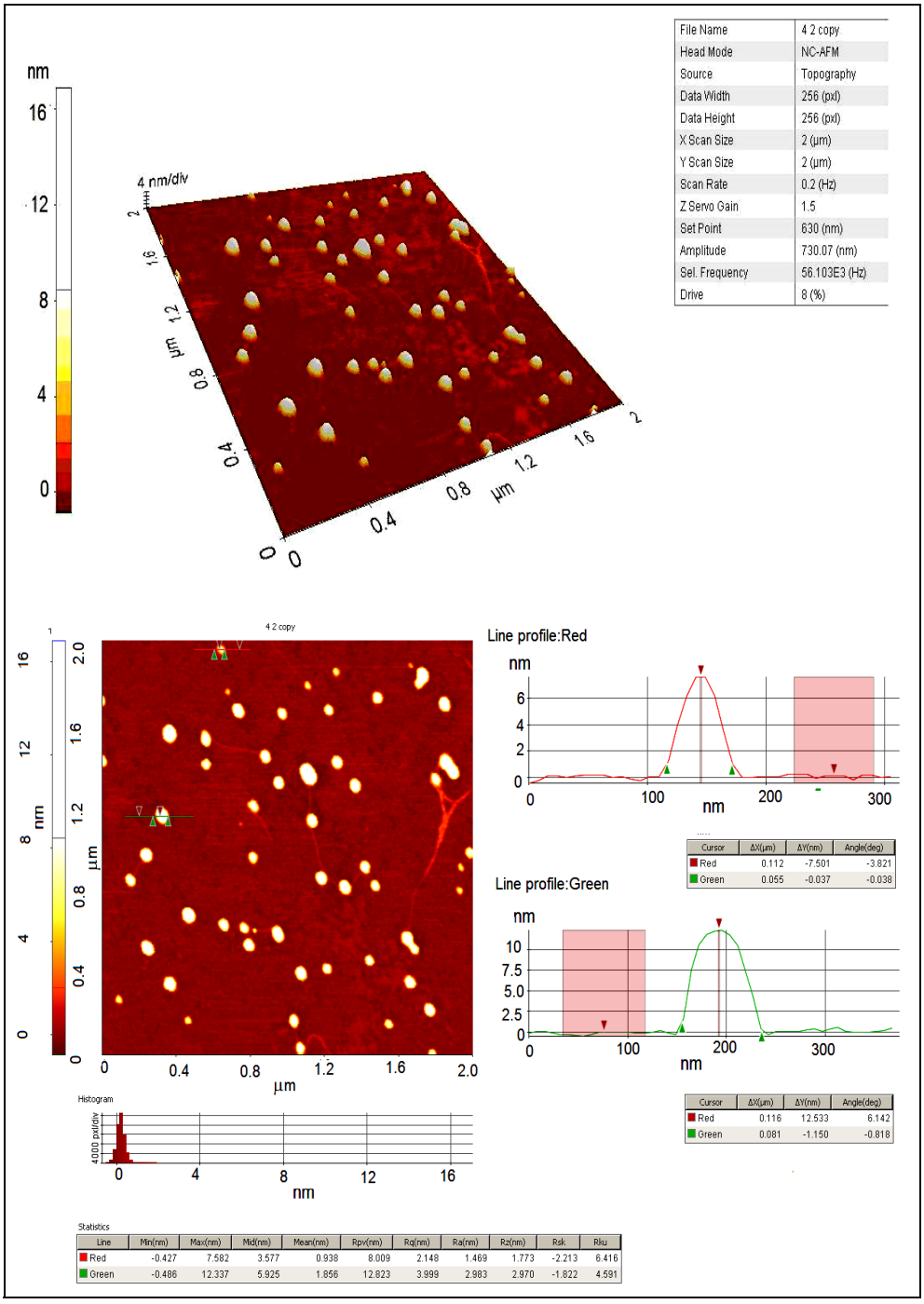

Fig. 4a – AFM scanning results for CoFe-CA aged sample (2 µm × 2 µm).

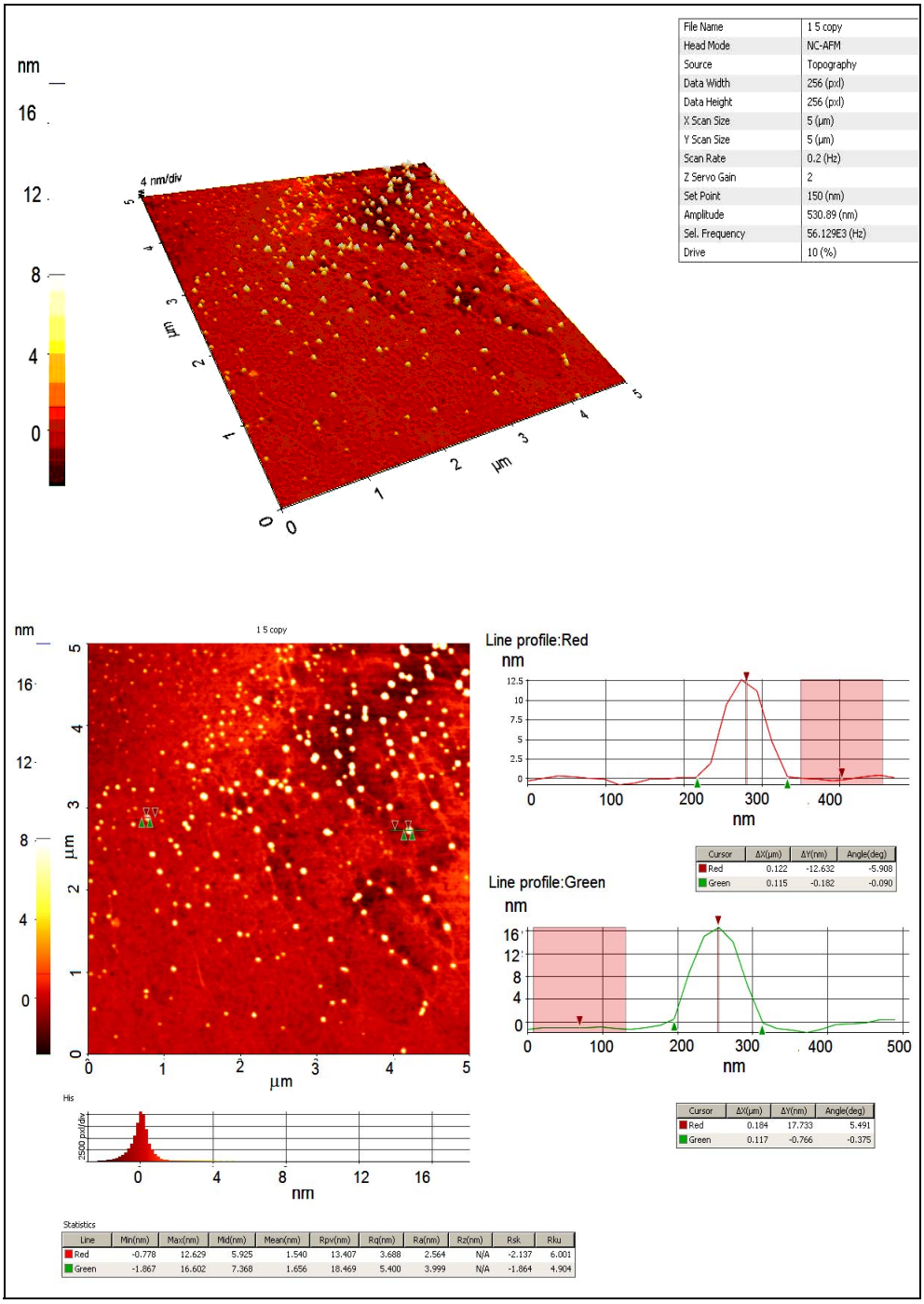

Fig. 4b – AFM scanning results for CoFe-SO aged sample (5 µm × 5 µm).

The aged suspensions were clearly affected by agglomeration and sedimentation, the analyses being possible after dilution and mixing at room temperature. The TEM images (Fig. 3a, b) were focused on the identification of still non-aggregated particles among groups of associated particles that seems also to be overlapped on the grid support. The mean diameters were found to be of 27.1 nm for CoFe-CA MNPs and 25.3 nm for CoFe-SO MNPs.

To get alternative insight on nanostructures topology we carried out AFM screening (Fig. 4a, b) with focus on larger nanostructures, according to the tapping tip sensitivity. AFM resolution being suitable for 3D imaging of relatively large particles as well as aggregates, from Figs. 4a, b, one can see similar values of particle height of 12 to 16 nm in both AFM images. Also, one can see that approximately 100 nm values characterize the diameter of both the CoFe-SO MNPs sample and CoFe-CA MNPs one (green line profile). We noticed that the scales are different (2 μm × 2 μm and respectively 5 μm × 5 μm). Thus the 2 μm × 2 μm AFM image in Fig. 4a, allowed observing better that aggregates are not spherical but more similar to ellipsoidal objects. Taking into account TEM and AFM observation, SANS investigation was carried out also on aged suspensions.

Following SANS experimental session, we could extract data only for CoFe-CA MNPs that remained homogeneous during recording procedure (Fig. 5a).

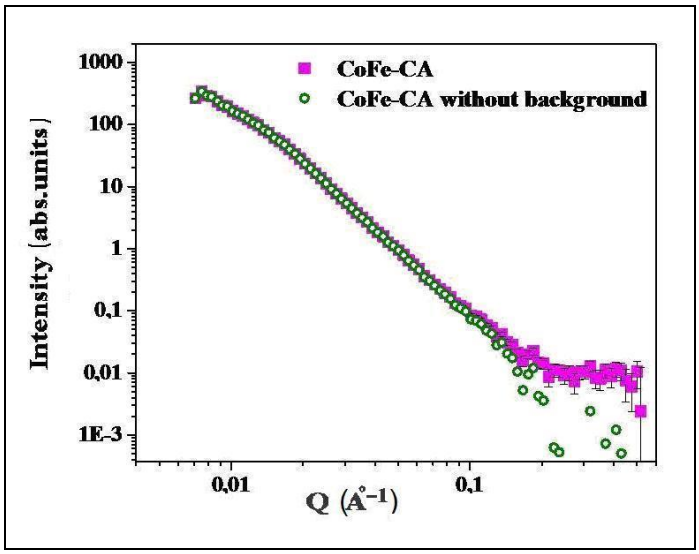

Fig. 5 – a) SANS recorded data for CoFe-CA aged sample (log-log scale); intensity (abs. units) *versus* scattering vector, Q (Å^{-1}): (i) original data (magenta squares); (ii) data without the background.

First theoretical approach (formulae (5), (6), (7)) was based on the fact that the shape of experimental curve as well as microscopy observations suggested distinct

mathematical fitting for three Q domains: 0.007 ÷ 0.03 Å^{-1} (domain I); 0.03 ÷ 0.06 Å^{-1} (domain II); 0.06 ÷ 0.15 Å^{-1} (domain III) (Fig. 5b).

$$I(Q) = A\int_0^1\int_0^1 \Phi^2(t)\,dx\,dy + B \tag{5}$$

$$\Phi(t) = 3\frac{\sin t - t\cos t}{t^3} \tag{6}$$

$$t = Q\left[a^2\cos^2\frac{\pi x}{2} + b^2\sin^2\frac{\pi x}{2}(1-y^2) + c^2y^2\right]^{\frac{1}{2}} \tag{7}$$

where $I(Q)$ is the scattering intensity, Q is the scattering vector, B is the background, and A is a coefficient connected with the background.

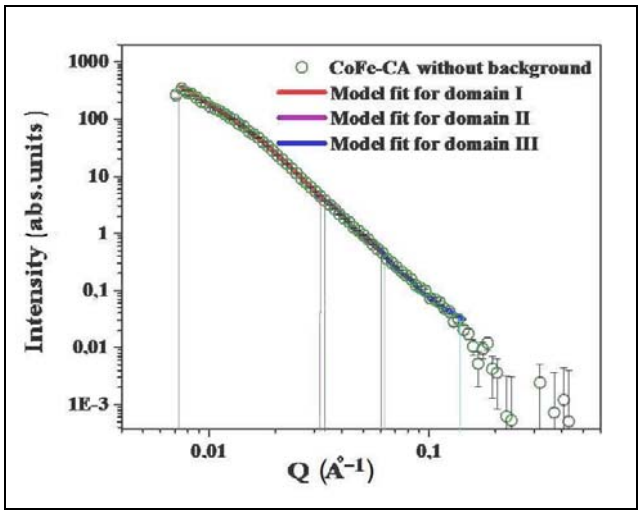

Fig. 5b – SANS theoretical fitted data in the range 0.007 < Q < 0.15 Å^{-1} for CoFe-CA aged sample (log-log scale); intensity (abs. units) *versus* scattering vector, Q (Å^{-1}) for three Q domain: 0.007 ÷ 0.03 Å^{-1} (domain I); 0.03 ÷ 0.06 Å^{-1} (domain II); 0.06 ÷ 0.15 Å^{-1} (domain III).

The corresponding ellipsoidal structures, *i.e.* the theoretical scatters within the colloidal aged samples, resulted to be two kinds of ellipsoids with the next nanosized dimensions on the three axes: a_1 = 67.4 nm; b_1 = 85.3 nm; c_1 = 9.6 nm; a_2 = 209.2 nm; b_2 = 86.2 nm; c_2 = 14.2 nm; a_3 = 204.3 nm; b_3 = 83.4 nm; c_3 = 14.3 nm (standard error was of 0.1 nm).

So, there are probably three populations of nanostructures defined by short chain aggregates, the last two ellipsoidal axes differing by one order of magnitude compared to those of the first theoretical ellipsoid. The interpretation, considering

implicitly mathematical approach and inherent limits, could be based on the hypothesis of short chain formation among neighbor nanoparticles in aged samples with eventual redistribution of coating shell, possibly with additional attached capping ions, released during precipitation of particle aggregates. There is still needed to be taken into account the hypothesis of surfactant excess [26] following precipitation of some aggregates [27, 28] that could release surfactant molecules from the connection sites during inter-particle junction formation. Thus, we conclude that the time stability of the analyzed samples is under one-year duration, although non-aggregated particles still remained in suspension according to TEM images of aged samples.

The second mathematical approach was focused on the discoid particles model (Fig. 5c).

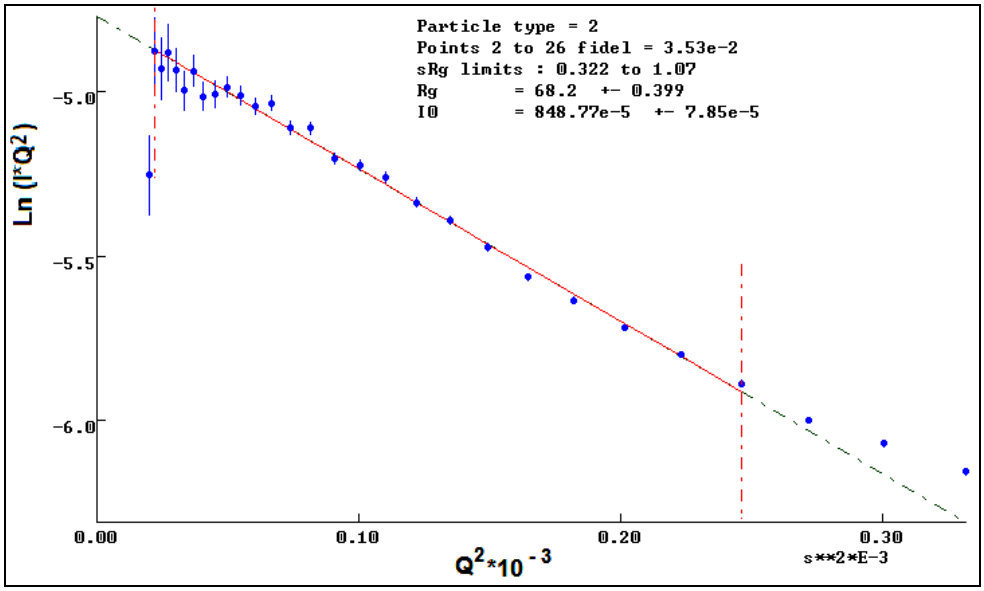

Fig. 5c – SANS data fitting by Guinier mathematical modeling.

This model (diluted sample, non-interacting scatters [29]) enabled us to get the theoretical flat particle radius from the radius of gyration, $R_g = 6.82 \pm 0.03$ nm, resulted from experimental data computation on the median part of the graph. Thus, in the real space $R_{max} = 1.41\ R_g = 9.62$ nm. This result is quite concordant with the value of c_1 axis – value of first type of ellipsoid provided by first mathematical modeling; it seems that actually there could be particles of 9 to 10 nm radius in the analyzed suspension and part of them associate as short chains geometrically approximated by ellipsoids.

In the last part of this paper we present the results obtained from biochemical assays carried out on aged MNP suspensions impact on wide spread environmental plants, of maize (*Zea mays* L.).

One can see in Fig. 6a, about 30% increase in the ratio chlorophyll A/ chlorophyll B (standard deviation of about 7%) which has the meaning of progressive stimulatory effect on the apparent photosynthesis efficiency [30–32] of CoFe-CA MNP suspensions. This could be related to the plantlets need of iron especially when they are grown in limited nourishing conditions. No significant variations were observed in the $(Chl\ A + Chl\ B) / (Chl\ A + Chl\ B + T.C.)$ ratio (standard deviation of about 8%), neither for CoFe-CA MNPs nor for CoFe-SO MNPs suspension (Fig. 6b). Also, in the case of chlorophyll ratio it seems that no effect for the tested range of MNP suspension concentration was evidenced in the case of CoFe-SO sample.

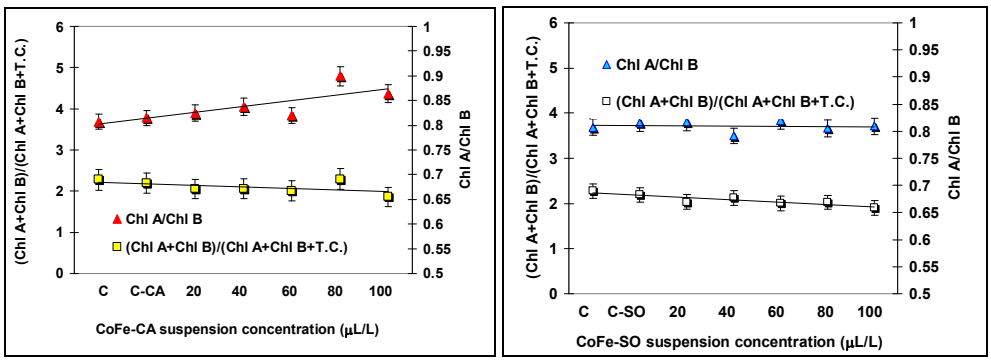

Fig. 6 – a (left) CoFe-CA influence on photosynthesis pigments in maize seedlings (C-control, only deionized water; C-CA – citric acid control); b (right) – CoFe-SO influence on photosynthesis pigments in maize seedlings (C-control, only deionized water; C-SO – sodium oleate control).

The results could be explained considering the different surface modifications of synthesized nanoparticles. When MNP cores were capped with citrate ions, then relatively thin shell of surfactant cover the iron oxide cores allowing the release of certain amount of catalytic iron and cobalt ions that enter the living cells interfering with cell biochemistry – as could be suggested by the photosynthesis pigment analysis. When oleate ions were surfacting metallic cores (fig. 7), then double coating shell was formed with first oleate ion shell bond with MNP metal ions at the magnetic core surface, while the second oleate shell formed interchain bonds with hydrophobic hydrocarbon tails of first oleate shell – thus carboxylic edges remaining orientated toward surrounding aqueous medium, ensuring MNP floating in suspension.

Because of such double layer formed from relatively long molecular structures arranged at the surface of MNP cores (Fig. 7), the release of significantly lower amount of catalytic metal ions is supposed to occur compared to single layer capped nanostructures, so that the bioeffect on cell biochemistry is reduced, practically not detectable at the level of photosynthesis pigment biochemical parameters. Next research step should be focused on the identification of stability duration of the two

kinds of samples by analyses carried out repeatedly at couple of months, at least by microscopy methods since SANS session schedule is less available and significantly more expensive. Also more detailed study of MNP bioeffects in early growth stage plantlets should be carried out aiming the evidence of nanotoxicity for certain concentrations.

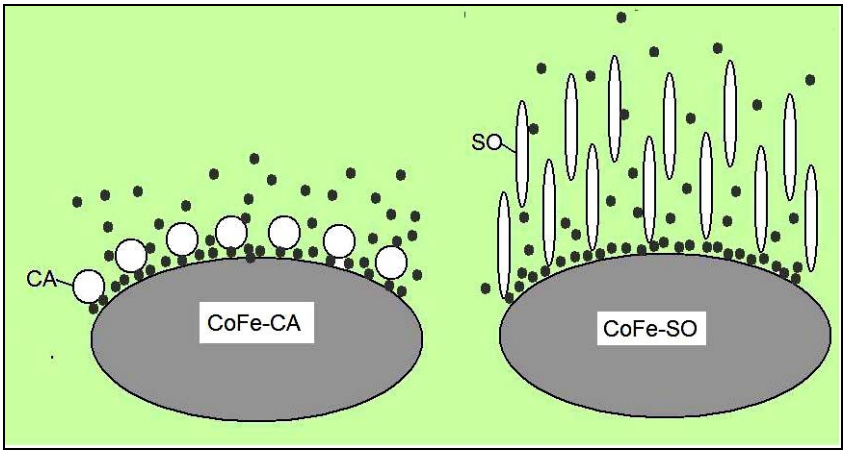

Fig. 7 – Metal ion release at the surface of CoFe-CA MNPs, capped with citrate (CA) single layer and at the surface of CoFe-SO MNPs, capped with oleate (SO) double layer.

5. CONCLUSION

For both MNP samples, crystallinity properties were preserved over time but different granularity properties were emphasized in time as shown by microscopy data and SANS experimental measurements. Although fine granularity of freshly prepared suspensions appeared to promise good stability in time for both types of samples, however, the surface modifying molecules induced differences between them. Citrate single layer stabilization was found to be more efficient than oleate double layer one. Still, in the one-year aged sample there are frequent aggregates, rather ellipsoidal shaped that should be avoided by using the samples within first couple of months. SANS data modeling evidenced possible short chains of ellipsoidal structures having smaller ellipsoid axis equal to the radius of non-associated, free, particles. The complementary study of MNP diluted suspension influence on plant photosynthesis pigments has evidenced slight stimulatory effect for citrate capped MNPs in contrast with the missing effect in the case of oleate shell coated MNPs.

Acknowledgements. We thank dr. Antoniu Moldovan from National Institute for Laser, Plasma and Radiation Physics, Bucharest, Romania for technical assistance in AFM measurements. The reported study was partially supported by RO-JINR Projects of 2018 year (Theme 04-4-1121-15/20).

REFERENCES

1. R. Kaiser, G. Miskolczy, IEEE Trans. on Magn. **6**, 694 (1970).
2. R. Ravaud, G. Lemarquand, V. Lemarquand, Tribol. Int. **43**, 76 (2010).
3. M. Imran, A. H. Shaik, A. R. Ansari, A. Aziz, S. Hussain, A. F. F. Abouatia, A. Khan, M. R. Chandan, RSC Adv. **8**, 13970 (2018).
4. R. Massart, IEEE Trans. Magn. **17**, 1247 (1981).
5. A. Goodarzi, Y. Sahoo, M. T. Swihart, P. N. Prasad, Mat. Res. Soc. Symp. Proc. **789**, 6.6.1 (2004).
6. N. Tran, T. J. Webster, J. Mater. Chem. **20**, 8760 (2010).
7. M. Mahdavi, M. B. Ahmad, M. J, Haron, F. Namvar, B. Nadi, M. Z. A. Rahman. J. Amin, Molecules **18**, 7533 (2013).
8. R. P. Araújo-Neto, E. L. Silva-Freitas, J. F. Carvalho, T. R. F. Pontes, K. L. Silva, I. H. M. Damasceno, E. S. T. Egito, A. L. Dantas, M. A. Morales, A. S. Carri, J. Magn. Magn. Mater. **364**, 72 (2014).
9. K. S. Rao, G. S. V. R. K. Choudary, K. H. Rao, C. Sujathad, Proc. Mater. Sci. **10**, 19 (2015).
10. C. R. Stein, M. T. S. Bezerra, G. H. A. Holanda, J. André-Filho, P. C. Morais, AIP Adv. **8**, 056303 (2018).
11. A. P. Budnyk, T. A. Lastovina, 1. A. L. Bugaev, V. A. Polyakov, K. S. Vetlitsyna-Novikova, M. A. Sirota, K. G. Abdulvakhidov, A. G. Fedorenko, E. O. Podlesnaya, A. V. Soldato, J. Spectroscopy 1412563 (2018).
12. L. Ardelean, D. Fica, A. Fica, G. Nechifor, D. Dragu, C. Bleotu, UPB Sci. Bull., Series B **80**, 33 (2018).
13. R. E. Rosensweig, Ferrohydrodynamics, Cambridge University Press, New York, (1985).
14. J. R. Peralta-Videa, L. Zhao, M. L. Lopez-Moreno, G. de la Rosa, J. Hong, J. L. Gardea Torresdey, J. Hazard. Mater. **186**, 1 (2011).
15. X. Ma, J. Geiser-Lee, Y. Deng, A. Kolmakov, Sci. Total Environ. **408**, 3053 (2010).
16. A.O. Govorov, I. Carmel. Nano Lett. **7,** 620 (2007).
17. N. Jayarambabu, K. V. Rao, S. H. Park, V. Rajendar, Digest J. Nanomater. Biostruct. **13**, 903 (2018).
18. M. V. Khodakovskaya, M. H. Lahiani, Handbook of Nanotoxicology John Wiley & Sons **4**, 121 (2014).
19. R. Massart, IEEE Trans. Magn. **17**, 1247 (1981).
20. A. I. Kuklin, A. K. Islamov, V. I. Gordeliy, Neutron News, **16**, 16 (2006).
21. A. S. Kirilov, E. I. Litvinenko, N. V. Astakhova, S. M. Murashkevich, T. B. Petukhova, V. E. Yudin, V. I. Gordelii, A. K. Islamov, A. I. Kuklin, Instrument. Exp. Techn. **(**Pribory i tekhnika eksperimenta) **47**, 334 (2004).
22. A. G. Soloviev, T. N. Murugova, A. H. Islamov, A. I. Kuklin, J. Phys. Conf. Series **351**, 012027 (2012).
23. H. K. Lichtenthaler, A. R. Wellburn, Biochem. Soc. Trans. **11**, 591 (1983).
24. A. Patterson, Phys. Rev. **56**, 978 (1939).
25. E. Puscasu, L. Sacarescu, A. Domocos, C. Leostean, R. Turcu, D. Creanga, M. Balasoiu, Rom. J. Phys. **61**, 946 (2016).
26. V. I. Petrenko, M. V. Avdeev, V. L. Aksenov, L. A. Bulavin, L. Rosta, Solid State Phenom. **152**, 198 (2009).
27. V. L. Aksenov, M. V. Avdeev, M. Balasoiu, D. Bica, L. Rosta, G. Török, L. Vekas, J. Mag. Mag. Mater. **258,** 452 (2003).
28. M. Balasoiu, O. I. Ivankov, D.V. Soloviov, S.N. Lysenko, R.M. Yakushev, A-M. Balasoiu-Gaina, N. Lupu, J. Optoel. Adv. Mater. **17**, 1114 (2015).
29. O. Glatter, O. Kratky, Small Angle X-Ray Scattering, Academic Press (1982).
30. M. Racuciu, D. Creanga, Rom. J. Phys. **62**, 804 (2017).
31. N. Pariona, A. I. Martinez, H.M. Hdz-García, L. A. Cruz, A. Hernandez-Valdes, Saudi J. Biol. Sci. **24**, 1547 (2017).
32. G. V. Siva, L. F. J. Benita, Int. J. Adv. Res. Biol. Sci. **3**, 230 (2016).